Clinically Relevant Outcome Measures for the I307N Rhodopsin Mouse: A Model of Inducible Autosomal Dominant Retinitis Pigmentosa

Michael T. Massengill,[1] Brianna Young,[2] Deep Patel,[1] Farwa Jafri,[1] Ernesto Sabogal,[1] Neil Ash,[1] Hong Li,[1] Cristhian J. Ildefonso,[2] and Alfred S. Lewin[1]

[1]Department of Molecular Genetics and Microbiology, University of Florida College of Medicine, Gainesville, Florida, United States
[2]Department of Ophthalmology, University of Florida College of Medicine, Gainesville, Florida, United States

Correspondence: Alfred S. Lewin, Department of Molecular Genetics and Microbiology, University of Florida College of Medicine, 1200 Newell Drive, Gainesville, FL 32610, USA; lewin@ufl.edu.

Submitted: July 20, 2018
Accepted: September 24, 2018

Citation: Massengill MT, Young B, Patel D, et al. Clinically relevant outcome measures for the I307N rhodopsin mouse: a model of inducible autosomal dominant retinitis pigmentosa. *Invest Ophthalmol Vis Sci*. 2018;59:5417–5430. https://doi.org/10.1167/iovs.18-25345

Purpose. The I307N rhodopsin (*Rho*) mouse is a light-inducible model of autosomal dominant retinitis pigmentosa (adRP) that may be useful in testing therapies. We investigated the time-course of retinal changes of the I307N *Rho* mouse with spectral-domain optical coherence tomography (SD-OCT).

Methods. SD-OCT was performed up to day 30 after light damage; electroretinography (ERG) was employed to evaluate photoreceptor function. We utilized ImageJ to analyze reflectivity of the retina. We used light and electron microscopy to assess retinal organization. We stained synaptophysin and zonula occludins-1 with immunohistochemistry to determine injury to the plexiform layers and retinal pigment epithelium (RPE). We performed lectin staining to evaluate retinal blood vessels.

Results. Retinal degeneration increased with longer exposures to light. An increase in retinal thickness was detected by SD-OCT on day 1 after light challenge followed by loss of the outer nuclear layer (ONL) by day 8. Degeneration was most severe in the nasal and inferior retina. Hyper-reflectivity on SD-OCT developed as early as 1 day after light exposure. Disorganization of the ONL, condensation of photoreceptor chromatin, disruption of the outer limiting membrane, and disarray of outer segments were associated with the hyper-reflectivity. Retraction of the outer plexiform synapses and resorption of the subretinal detachment contributed to retinal thinning. The RPE remained intact, whereas atrophied major retinal vessels were evident after light damage.

Conclusions. Our time-course analysis of retinal degeneration in the I307N *Rho* mouse with SD-OCT and other outcome measures should enable the use of the mouse model in preclinical efficacy studies and mechanistic studies.

Keywords: retinitis pigmentosa, rhodopsin, SD-OCT, electroretinography, hyper-reflectivity

Retinitis pigmentosa (RP) is a group of retinal dystrophies in which apoptosis of rod photoreceptors is followed by a secondary wave of cone death. The 1.5 million patients worldwide who are afflicted with RP typically exhibit impaired dark adaption and loss of peripheral vision in adolescence, which can progress to complete blindness in a minority of cases.[1] Mutations in over 80 genes, and even diverse mutations within a single gene such as the 204 disease-causing mutations identified in human rhodopsin (*RHO*), can lead to RP.[1–3] This complex genetic landscape presents a formidable barrier to understanding RP pathogenesis and to generating therapies.[4] An additional obstacle in progressing potential therapies from the bench to the bedside relates to weaknesses of RP mouse models. The inducible and rapid retinal degeneration exhibited by the I307N *Rho* mouse presents an alternative platform that may complement the study of RP.[5,6]

The I307N *Rho* mouse model, whose alias of Tvrm4 reflects the core facility in which it was discovered, was established by the Nishina group via chemical mutagenesis, garnering attention due to its development of retinal pigmentation after repeated exposure to light during ophthalmoscopy.[5] The I307N mouse *Rho* mutation was identified as the cause of retinal degeneration, which only occurs with exposure to bright—but not ambient—light. Importantly, the I307N *Rho* mouse recapitulates some features of the class B1 phenotype of mutant autosomal dominant RP (adRP) caused by mutations in *RHO* in humans, including impaired dark adaptation and focal degeneration with areas of preserved retina.[5–7] In addition, glial reactivity and death of cones, which are general or late-stage features of RP, occur in the retina of the I307N *Rho* mouse after illumination with bright light.[6]

Many mouse models of RP—including the *rd1*,[8] *rd10*,[8] and T17M *RHO*[9] mice—are imperfect because their early rod loss is consistent with disease onset in infancy[10] rather than adolescence, as seen in humans.[5,6] Study of retinal degeneration in these mice may even be confounded by early disease onset because eye development in mice extends into the postnatal period.[6,11] Additionally, the phenotype of transgenic RP mouse models may arise, in part, from transgene overexpression rather than the activity of the mutated gene alone.[12] Furthermore, other RP mice may be impractical in the setting of preclinical efficacy studies, as early onset of retinal degenera-

tion challenges the speed with which a gene therapy or pharmacological intervention can achieve maximal therapeutic effect.[13] Conversely, testing in mice with a protracted disease course, like the P23H *RHO* transgenic or P23H *Rho* knock-in mice, is costly and inefficient, especially for initial proof-of-concept studies.[14,15] The I307N *Rho* mouse circumvents these considerations because it expresses physiologic levels of rhodopsin[5,16] and the light-inducible phenotype enables delay of disease onset into adulthood or after achieving a therapeutic effect with intervention.

Inducible and rapid retinal degeneration occurs in the I307N *Rho* mouse only after exposure to bright light, providing a highly controllable setting where RP pathogenesis can be dissected or putative therapies can be tested. However, generation of a timeline of clinically relevant end points is necessary to organize an informative preclinical efficacy study or to dissect a specific disease process.[8,17,18] Spectral-domain optical coherence tomography (SD-OCT) has become an important methodology to follow the progression of retinal disease in mouse and human.[19,20] Therefore, we performed a time-course analysis of the acute and chronic SD-OCT changes that ensue in the I307N *Rho* mouse after exposure to bright light. We found that detectable loss of the outer nuclear layer (ONL) thickness by SD-OCT occurs predominantly during the first week after the light challenge and that the inferior and nasal retina is impacted more severely than the superior and temporal retina. We observed that the total retinal thickness continued to diminish 2 weeks after light injury due to resolution of the subretinal void left by the vacated photoreceptors, retraction of the synapses of the outer plexiform layer (OPL), and additional clearance of the ONL that is not easily discernable by SD-OCT. Additionally, an acute period of hyperreflectivity developed rapidly in the SD-OCT B-scan during the first week after light injury, which achieved a higher intensity in the nasal retina compared to temporal retina. Despite substantial retinal deterioration, the retinal pigment epithelium (RPE) remained functionally and histologically intact. However, the large retinal vessels atrophied within 2 weeks after exposure to light.

Results

Retinal Degeneration Varies With Exposure Time to Light

The protocol employed by the Nishina group[5] in the initial characterization of the I307N *Rho* mouse involved overnight dark adaptation, pupil dilation, and exposure of conscious mice to 12,000 lux of achromic light for up to 5 minutes in a cage equipped with mirrored walls. In generating a light damage protocol to induce retinal degeneration in anesthetized I307N *Rho* mice, we tested various sources, intensities, and durations of light with limited success. We found that an intensity of 20,000 lux of light for 10 minutes was insufficient to generate photoreceptor cell death in anesthetized mice (unpublished data, 2017). During the course of our study, Gargini et al.[6] corroborated the findings made by the Nishina group. They also reported that anesthetized I307N *Rho* mice are resistant to light damage and suggested that intact eye movements may be necessary to induce retinal degeneration. Others have also found that anesthetic cocktails containing ketamine and xylazine may be neuroprotective in the setting of light damage.[21]

To avoid issues related to anesthesia, we explored the use of cages equipped with a light source fastened to the roof to initiate retinal degeneration in the conscious and freely mobile mouse[22] (Supplementary Fig. S1A). To identify the appropriate dose of light to induce a significant and reproducible loss of ONL thickness, I307N *Rho* mice were exposed in the cages to either no light or 20,000 lux of white LED-light for 10, 20, or 30 minutes (Supplementary Fig. S1B). Of note, I307N *Rho* mice were not averse to the 20,000 lux light. Baseline, 1- and 2-week post-light damage SD-OCT scans were obtained, and the ONL thickness was measured to observe whether there were any differences between the treatments.

I307N *Rho* mice that were subjected to light damage experienced significant decreases in ONL thickness that were dependent on the duration of exposure to light in the cages as well as the position in the retina with reference to the optic nerve head (ONH; Fig. 1A). In the 10-minute exposure group, significant loss of ONL thickness was observed in both the nasal and inferior retina, but the superior and temporal retina remained largely unaffected. When the duration of light increased to 20 minutes, the damage induced in the nasal and inferior retina became more severe, and the area of significant ONL loss extended to include the temporal and superior retina. Substantial loss of ONL thickness occurred along most of the horizontal and vertical axes in the SD-OCT frames corresponding to the 30-minute exposure group (Fig. 1B).

Full-field scotopic ERG data further indicated that longer durations of light exposure increase the extent of retinal degeneration in the I307N *Rho* mouse, as a- and b-wave amplitudes were smallest in the 30-minute exposure group (Supplementary Fig. S2A, S2B). Importantly, wild-type (WT) littermates challenged with 30 minutes of light did not display differences in ONL thickness (Supplementary Fig. S3A, S3B). Additionally, the ONL remained intact in I307N *Rho* mice that were not exposed to bright light over the same 1-month time period (Supplementary Fig. S2C).

Transient Swelling and Progressive Thinning After Light Damage

To understand the SD-OCT changes that occur after light challenge more completely, I307N *Rho* mice were subjected to the 30-minute light damage protocol, and SD-OCT was performed beforehand or on days 1, 3, 5, 8, 15, or 30 thereafter. The 30-minute duration was selected so that an observable phenotype would be elicited. Although all mice exhibited evidence of injury by OCT, there was a range of apparent damage, with the temporal and superior retina spared in some animals (Fig. 2A). This observation will be discussed below. A transient increase in retinal thickness was observed in the nasal and inferior retina 1 day after light damage, suggestive of retinal swelling. Resolution of swelling, or swelling counteracted by tissue loss, occurred by day 3 when the retinal thickness was only slightly less than baseline. Significant thinning of the retina began 5 days after the light challenge when the retinal quadrants appeared to be equally deteriorated. The decline in retinal thickness progressed from day 8 to day 15, with a reproducible pattern of greater retinal loss in the nasal and inferior quadrants compared to the temporal and superior quadrants. The nadir of retinal thickness was likely achieved before day 15, as further retinal loss was not apparent on day 30 (Fig. 2B).

The variable damage to the retina (Fig. 2A) may depend on the variable activity of individual I307N *Rho* mice. Mice at rest have a downward-tilting head position that focuses overhead light on the inferior and nasal retina. This posture likely accounts for the severe degeneration of the inferior and nasal retina in nearly all mice. However, highly active mice with dynamic eye and body movements may experience temporal and superior retinal injury via exposure to higher effective doses of light. One behavior in particular—standing erect on

Investigative Ophthalmology & Visual Science

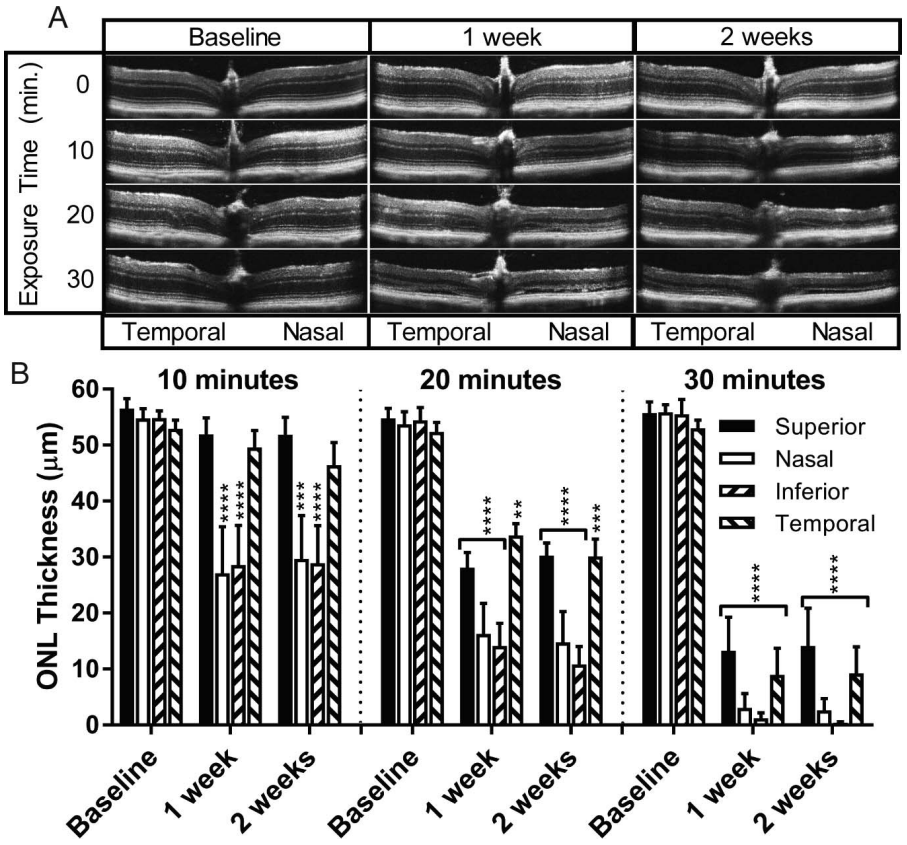

Figure 1. The extent of anatomical retinal degeneration increases with exposure time to light. Eight- to 12-week-old I307N *Rho* mice were subjected to either ambient light or 10, 20, or 30 minutes of 20,000 lux of light ($n = 5$ per group). SD-OCT B-scans were obtained approximately 2 weeks prior to as well as 1 and 2 weeks after light challenge. (**A**) Displayed are representative SD-OCT B-scans centered on the ONH, which encompass approximately 1.4 mm segment of retina. (**B**) ONL thickness was measured in micrometers (μm) in each retinal quadrant of the SD-OCT B-scans. One-way ANOVA for separate quadrants followed by multiple comparisons tests employing the baseline condition as the reference were utilized to determine statistical significance. $^{**}P < 0.01$; $^{***}P < 0.001$; $^{****}P < 0.0001$.

hind legs with an upward-tilting head—not only positioned the eyes closer to the light source but may have also focused the light on the temporal and superior retina.

Asymmetric Development of Hyper-Reflective Signal on SD-OCT

We observed areas of hyper-reflectivity between the OPL and the subretinal space in SD-OCT B-scans of the I307N *Rho* retina on days 1 through 5 after exposure to light (Fig. 2A), which were absent in light-exposed WT littermates (Supplementary Fig. S3A). Animals with obvious swelling demonstrated complete obscuring of the OPL, ONL, OLM, ISs, and OSs by a single band of hyper-reflective signal. Other animals showed two distinct bands of hyper-reflectivity. The first band obscured the OPL and inner portion of the ONL while the second disrupted the reflective patterning of the outer portion of the ONL, OLM, ISs, and OSs.

To better describe the changes in reflectivity that occurred with light damage, we used ImageJ (https://imagej.nih.gov/ij/, provided in the public domain by the National Institutes of Health, Bethesda, MA, USA) to generate longitudinal reflectivity profiles (Supplementary Figs. S4, S5).[23–25] Individual profiles corresponding to either the nasal or temporal retina at a given time point after induction of retinal degeneration were compiled to visualize the average changes that occur in eight I037N *Rho* mice (Fig. 3A, 3B). A drastic change in the shape of the reflectivity curve occurred on day 1, as the area of hyper-reflectivity between the positions corresponding to the OPL (approximately 75 μm) and RPE (approximately 220 μm) exhibited reflectivity values that were abnormally positive when compared to the normally hyporeflective signal of the naïve condition. With progression to day 3, the area of hyper-reflectivity exhibited lower values while occupying approximately the same space. Retinal thinning was noted on day 5 and even further on day 8 after damage, when a new reflectivity spike appeared that likely signified the abnormal juxtaposition of the OPL and the OLM after ONL loss (Supplementary Fig. S4).

Since we had observed that the extent of retinal thinning was greater in the nasal versus temporal retina (Fig. 2), we hypothesized that the intensity of reflectivity in the nasal retina would exceed that of the temporal. Therefore, we measured, in individual profiles, the area under the curve (AUC) within a defined area of hyper-reflectivity (Fig. 3C) encompassing the OPL, ONL, and a portion of the subretinal space. Analysis was limited to the baseline, day 1, and day 3 conditions when the area of hyper-reflectivity aligned substantially. Reflectivity increased disproportionately in the nasal versus temporal retina on day 1 after light challenge, before both areas decreased to a similar value by day 3. We thus concluded that the nasal retina undergoes a more pronounced period of hyper-reflectivity that may be predictive of future ONL loss.

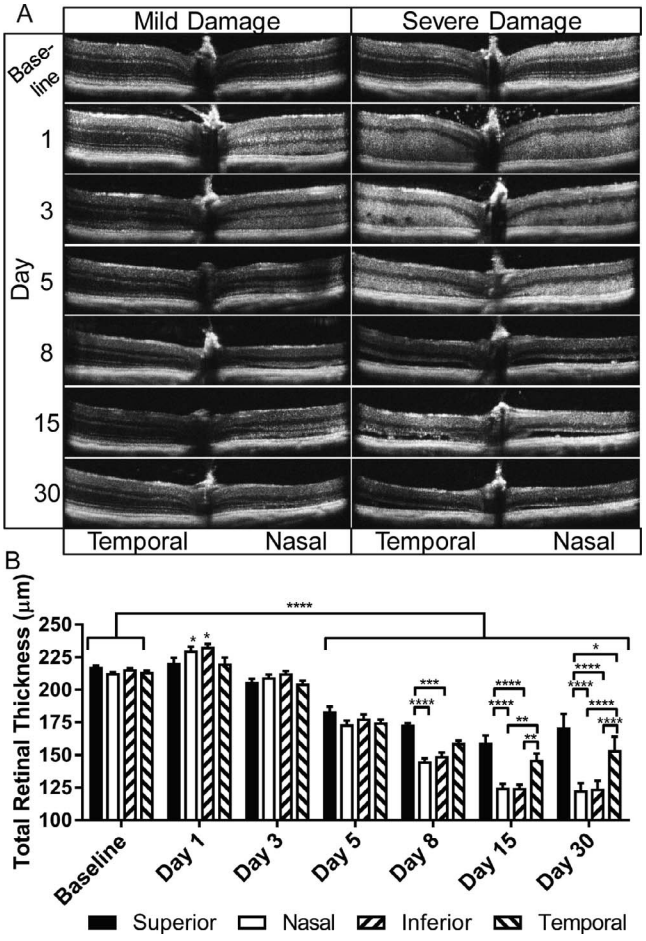

Figure 2. Acute and chronic SD-OCT changes of the I307N *Rho* mouse. Eight- to 12-week-old I307N *Rho* mice were exposed to 30 minutes of 20,000 lux of light. SD-OCT was performed before or 1, 3, 5, 8, 15, or 30 days thereafter ($n = 8$ per group, except for day 15, where $n = 7$). The data do not represent a time-course of changes for a single mouse since repeated administration of anesthesia would be harmful, and mice were euthanized for postmortem analysis. Mice in the day 5 group were an exception and were re-imaged for the day 15 or 30 groups. (**A**) A spectrum of severity of retinal degeneration was observed in the I307N *Rho* mouse challenged with the same light damage protocol. Provided are representative SD-OCT B-scans captured at each time point corresponding to mice experiencing either mild or severe retinal degeneration. (**B**) The total retinal thickness was measured as the distance in micrometers (μm) from the NFL to the RPE in the SD-OCT B-scans. Measurements were performed in the superior, inferior, nasal, and temporal quadrants of the retina. The *bar graph* represents the mean ± SEM. Two-way ANOVA followed by multiple comparisons tests was utilized to determine statistical significance. $^{*}P < 0.05$; $^{**}P < 0.01$; $^{***}P < 0.001$; $^{****}P < 0.0001$.

Light-Induced Disarray of the OLM, ONL, and Subretinal Space

The hyper-reflectivity observed in SD-OCT scans of the retina on days 1 and 3 may represent a pathologically relevant process. This signal has been proposed to arise due to the refractive changes that occur in photoreceptors during apoptosis.[24,26] The normal organization and wave-guiding nature of the retina may also be disturbed by swelling in the acute period following light damage[27] (Fig. 2). To better view retinal architecture, plastic sections of samples obtained during the first week following induction of retinal degeneration were analyzed by light microscopy (Fig. 4A). On days 1 and 3, the

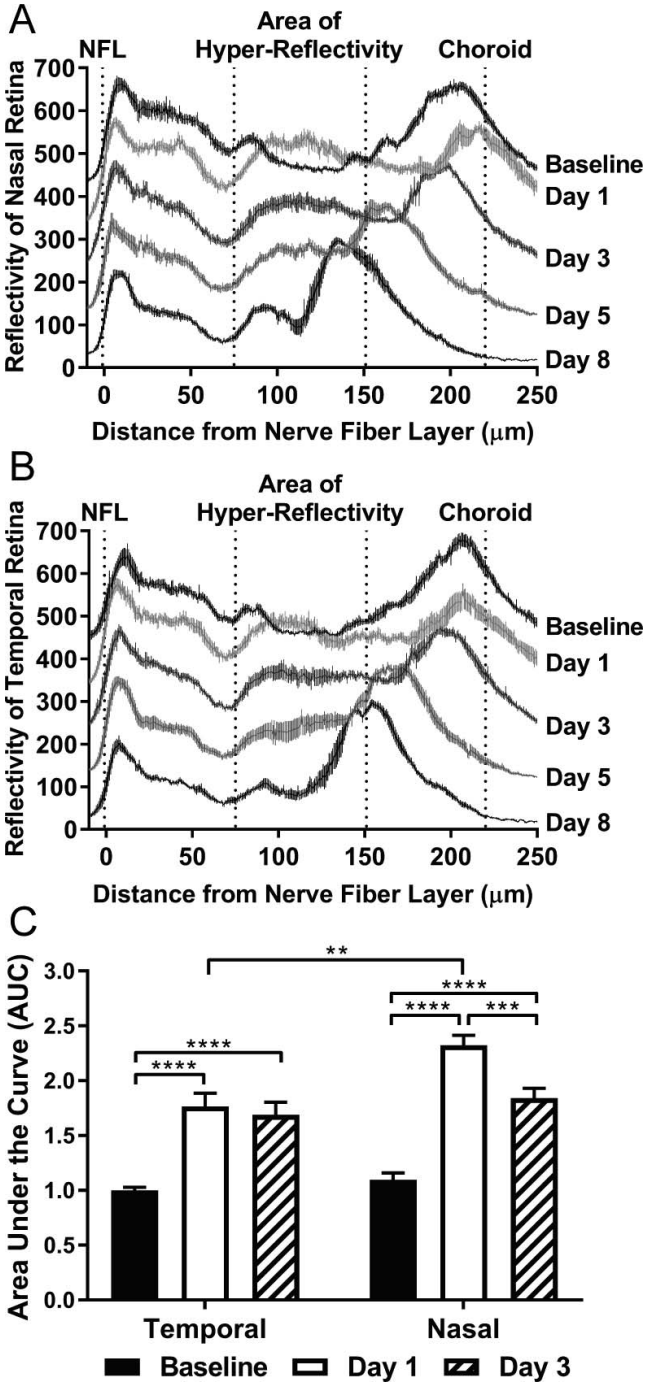

Figure 3. SD-OCT associated hyper-reflectivity is asymmetric and peaks one day after light damage. Longitudinal reflectivity profiles for $n = 8$ mice were generated and combined to create composite curves describing the (**A**) nasal and (**B**) temporal retina for the baseline, as well as days 1, 3, 5, and 8 post-light damage time points. Composite curves are represented as the mean reflectivity ± SEM at a given position along the retina. The curves corresponding to each time point are offset by 100 units on the Y-axis so that the differences in deflection can be appreciated between time points. The area of hyper-reflectivity is marked as spanning approximately from the INL to subretinal space. (**C**) The area under the curve (AUC) was measured within the area of hyper-reflectivity in individual reflectivity plots of the temporal or nasal retina for the baseline, as well as day 1 and day 3 post-light damage time points. The *bar graph* represents the mean AUC ± SEM ($n = 8$ per time point). Two-way ANOVA followed by multiple comparisons tests was utilized to determine statistical significance. $^{**}P < 0.01$; $^{***}P < 0.001$; $^{****}P < 0.0001$.

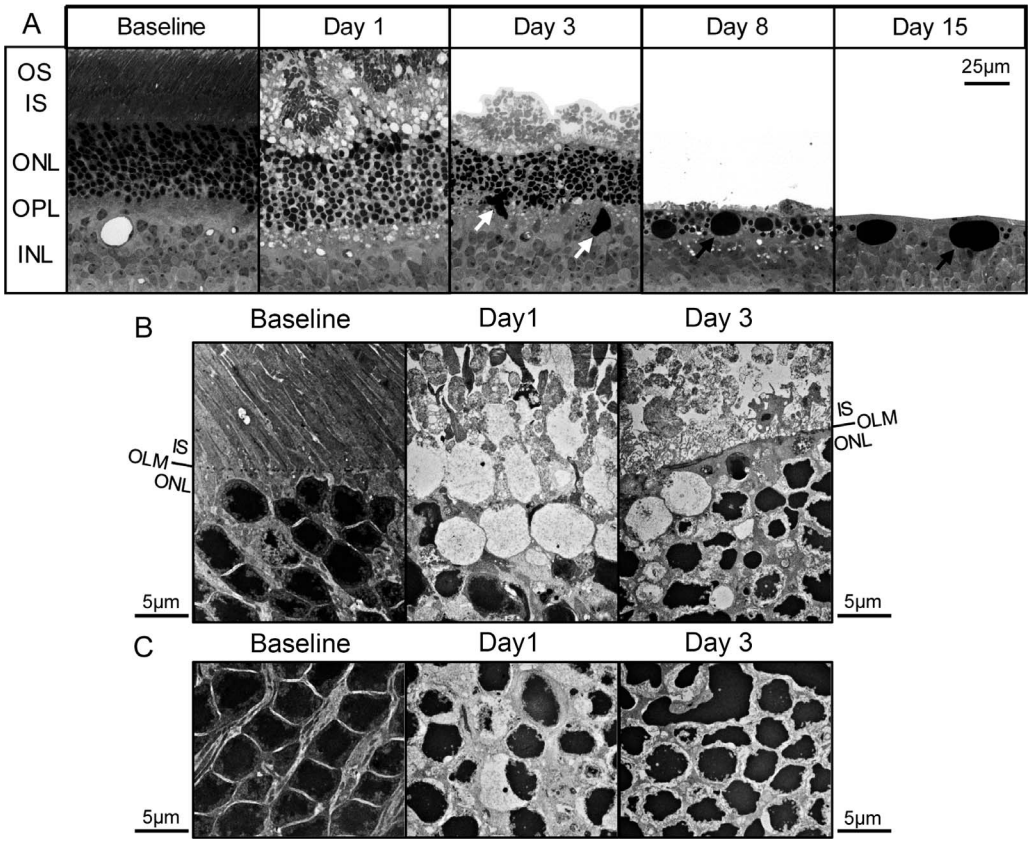

Figure 4. Light-induced alterations in photoreceptor nuclei and ONL. Plastic sections were obtained from retinas of I307N *Rho* mice before and 1, 3, 8, or 15 days after exposure to 20,000 lux of light for 30 minutes. (**A**) Representative visual fields with an original magnification of 40× are displayed. Unlike the samples from the day 3 and day 8 time points that contained subretinal detachments, the RPE was adherent to the ONL in the day 15 sample. The RPE was cropped out of images for simplicity. *White arrows*: large pleomorphic nuclear material. *Black arrows*: large spherical nuclear material. (**B**, **C**) Representative visual fields are displayed with an original magnification of 5000× of the: (**B**) interface between the ONL and subretinal space, and the (**C**) ONL. (**B**) Obliteration of the OLM was apparent by day 1 after light exposure. The ONL was separated from the inner segments by nuclei-free spaces surrounded by membrane or ECM. Deposition of dense ECM in the ONL occurred by day 3 and contributed to a newly formed demarcation between the ONL and subretinal space. (**C**) The normal configuration of chromatin at baseline was replaced by condensed chromatin consistent with apoptosis. The tight packing of the photoreceptor nuclei was disrupted, especially on day 1.

ONL, as well as the inner plexiform layer (IPL) and subretinal space, displayed a wavy configuration in areas near the ONH. This appeared to disrupt the longitudinal packing of nuclei, as nuclei-free white space was observed. Residual outer segments were observed as clumps in the subretinal space one day after light challenge, an observation also reported by Budzynski et al.[5] These were replaced by punctate material by day 3. Densely staining pleomorphic globules (*white arrows*), perhaps composed of phagocytosed nuclear debris associated with microglia, were observed in the ONL, OPL, and inner nuclear layer (INL) on day 3. By days 8 and 15, the dense globules were spherical and appeared similar to structures reported by Gargini et al.[6] and Budzynski et al.[5] (*black arrows*). Interestingly, the ONL and OPL were almost absent by day 15.

We next performed electron microscopy to visualize the changes to the microstructure of the I307N *Rho* retina during the acute phase of light-induced degeneration (Fig. 4B, 4C). The OLM was obliterated 1 day after exposure to bright light, which would allow the flow of fluid between the subretinal space and the ONL. By day 3, a linear demarcation between the subretinal space and ONL had reformed. This demarcation appeared to be formed by the deposition of dense extracellular matrix (ECM) that surrounded the photoreceptor nuclei rather than by an organized OLM. Additionally, on day 1, the normal juxtaposition of the ONL and photoreceptor inner segments (ISs) was interrupted by fluid-filled droplets enclosed by membrane or ECM. These structures, which were also observed at the day 3 time point, may represent ghosts of dying photoreceptor cell bodies after their phagocytosis by microglia and may produce the enhanced reflectivity in SD-OCT[28] (Fig. 4B). Furthermore, photoreceptor nuclei of the baseline condition displayed condensed central chromatin, which is typical of rod photoreceptors of nocturnal mammals, such as mice, and permissive to the transmission of light.[29,30] Pan-nuclear condensation and fragmentation of chromatin were evident in many nuclei on days 1 and 3 time points, which suggested that apoptosis was a major pathway leading to photoreceptor cell death in the I307N *Rho* mouse (Fig. 4C). Interestingly, these effects are remarkably similar to the phenotype of the arrestin$^{-/-}$ mouse that also experiences retinal degeneration with exposure to light.[24] Taken together, the dissolution of the OLM, pyknosis of photoreceptor nuclei, disappearance of photoreceptor cell bodies, and deposition of ECM likely contributed to the hyper-reflectivity observed on SD-OCT.

Reduction in the Synaptic Density of the OPL and Area of the Subretinal Void

We found that the loss of ONL detected by SD-OCT occurred almost exclusively during the first week following light injury,

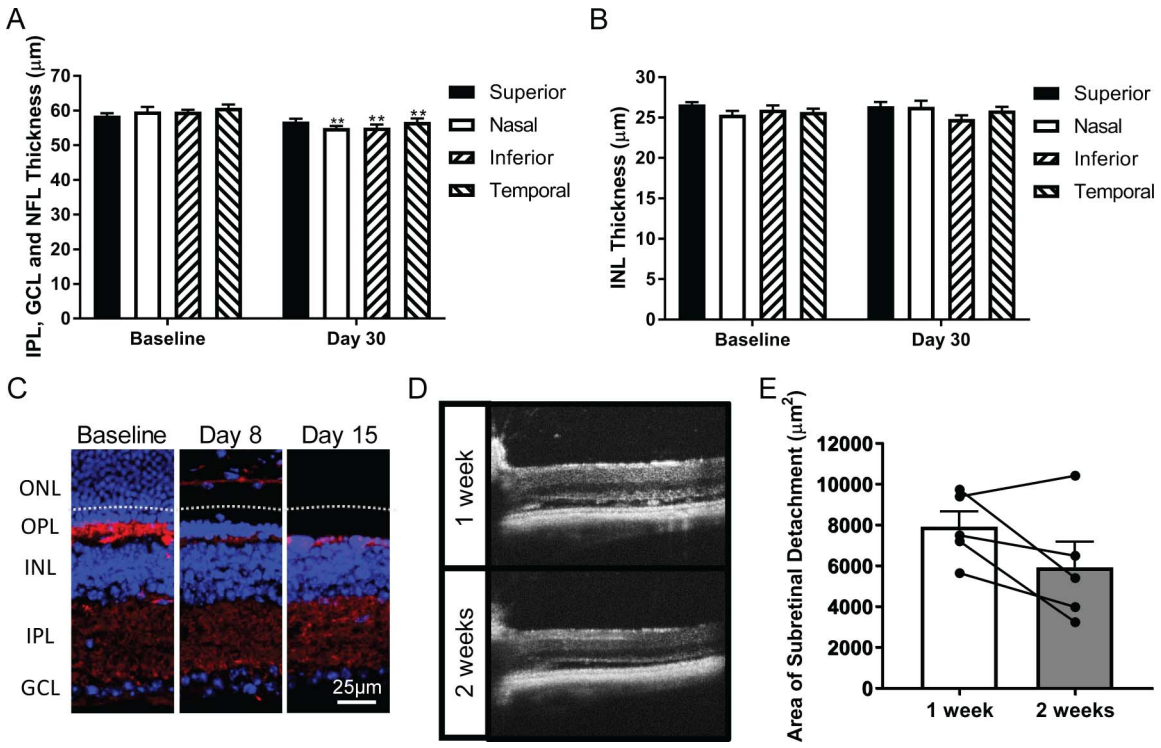

Figure 5. Resorption of the OPL and subretinal void contribute to retinal thinning. (**A**) The combined IPL, GCL and NFL thickness, as well as (**B**) INL thicknesses were measured in micrometers (μm) in SD-OCT B-scans captured from baseline and day 30 post-light damage I307N *Rho* mice ($n = 7$). *Bar graphs* represent the mean layer thickness of a particular quadrant ± SEM. Non-paired two-tailed Student's *t*-tests were performed to assay for statistical significance. (**C**) Immunohistochemistry staining with anti-synaptophysin (*red*) and DAPI (*blue*) was performed to assess the density and thickness of the OPL. Displayed are representative fluorescence micrographs with original magnifications of 40×. The *white dashed line* shown in day 8 demarcates the separation between the subretinal space and the RPE. We also noted that the anti-mouse secondary antibody stained blood vessels. (**D**) Representative SD-OCT B-scans of the nasal retina depicting the subretinal detachment 1 week and 2 weeks after light exposure. (**E**) SD-OCT B-scans that contained obvious retinal detachment from the 30-minute exposure group in the initial dose response experiment were included for analysis ($n = 5$ eyes). The area of the subretinal detachment was measured in a 650 μm segment of the nasal retina at weeks 1 and 2 post-light challenge. The graph depicts the mean area of the subretinal detachment (μm^2) ± SEM. Paired measurements for a single eye across the two time points are joined by a line segment. A two-tailed paired Student's *t*-test with a threshold of $P = 0.05$ was utilized to determine statistical significance.

yet the retina continued to thin by approximately 25 μm in the inferior and nasal retina thereafter. Inner retinal remodeling, which has been reported in the I307N *Rho* mouse,[6,31] may contribute to this progressive loss. We detected only minor decreases in the thicknesses of a combined layer encompassing the NFL, GCL and IPL, as well as the INL (Fig. 5A, 5B), in the SD-OCT scans associated with I307N *Rho* mice 30 days after exposure to light. We were unable to measure the depth of the OPL via SD-OCT due to its abnormal juxtaposition with and obscuring by the OLM. We therefore analyzed the density of the synaptophysin-positive synapses of the OPL by immunohistochemistry. We found that the synaptic density of the OPL decreased substantially by day 8 following light injury while the synapses of the IPL were preserved (Fig. 5C). The secondary anti-mouse IgG antibody also stained blood vessels in these sections. Of note, the b-wave:a-wave ratio, a measure for the integrity of synaptic connection between photoreceptors and second-order neurons, was larger in the degenerating I307N *Rho* mouse compared to the naïve I307N *Rho* mouse, which suggested that the surviving synapses of the inner retina likely remain functionally intact[32] (Supplementary Fig. S2C). In agreement with the earlier light microscopy data (Fig. 4A), the ONL and OPL were nearly undetectable by day 15.

The rapid loss of photoreceptors created an acellular void in the outer retina in a subset of I307N *Rho* mice that was evident as a hypo-reflective space on SD-OCT (Fig. 5D). Reabsorption of the void may also contribute to the continued decline in retinal thickness. To test this hypothesis, we re-examined the SD-OCT B-scans captured from I307N *Rho* mice from the 30-minute exposure group in the initial dose response experiment (Fig. 2). We found that 5 of the 10 eyes demonstrated significant retinal detachment, and we subsequently measured the area of the subretinal detachment in the nasal retina at 1- and 2-weeks post-light damage. The area encompassing the subretinal void decreased in 4 of 5 eyes with time; however, the difference in means of the two groups was not significant (Fig. 5E). Accordingly, we conclude that collapse of the OPL, additional clearance of the ONL, and resorption of the subretinal detachment each make contributions to the decline in retinal thickness between the 1- and 2-week time points.

Functional Maintenance of RPE in the Face of Profound Photoreceptor Death

The rapid death of photoreceptors in the I307N *Rho* mouse after light injury likely exposed the RPE to toxic substances derived from photoreceptor debris and microglial activity, especially free radicals generated via NADPH oxidase.[33] Budzynski et al.[5] reported that retinal pigmentation is apparent on fundus examination of the I307N *Rho* mice. Therefore, we hypothesized that RPE atrophy may occur during the retinal degenerative process of the I307N *Rho* mouse.[5] To test whether the RPE in the I307N *Rho* mouse expressed signs of dysfunction after exposure to light, we performed immunohistochemistry on RPE whole mounts to visualize the tight junction protein zonula occludens-1 (ZO-1) that is enriched at

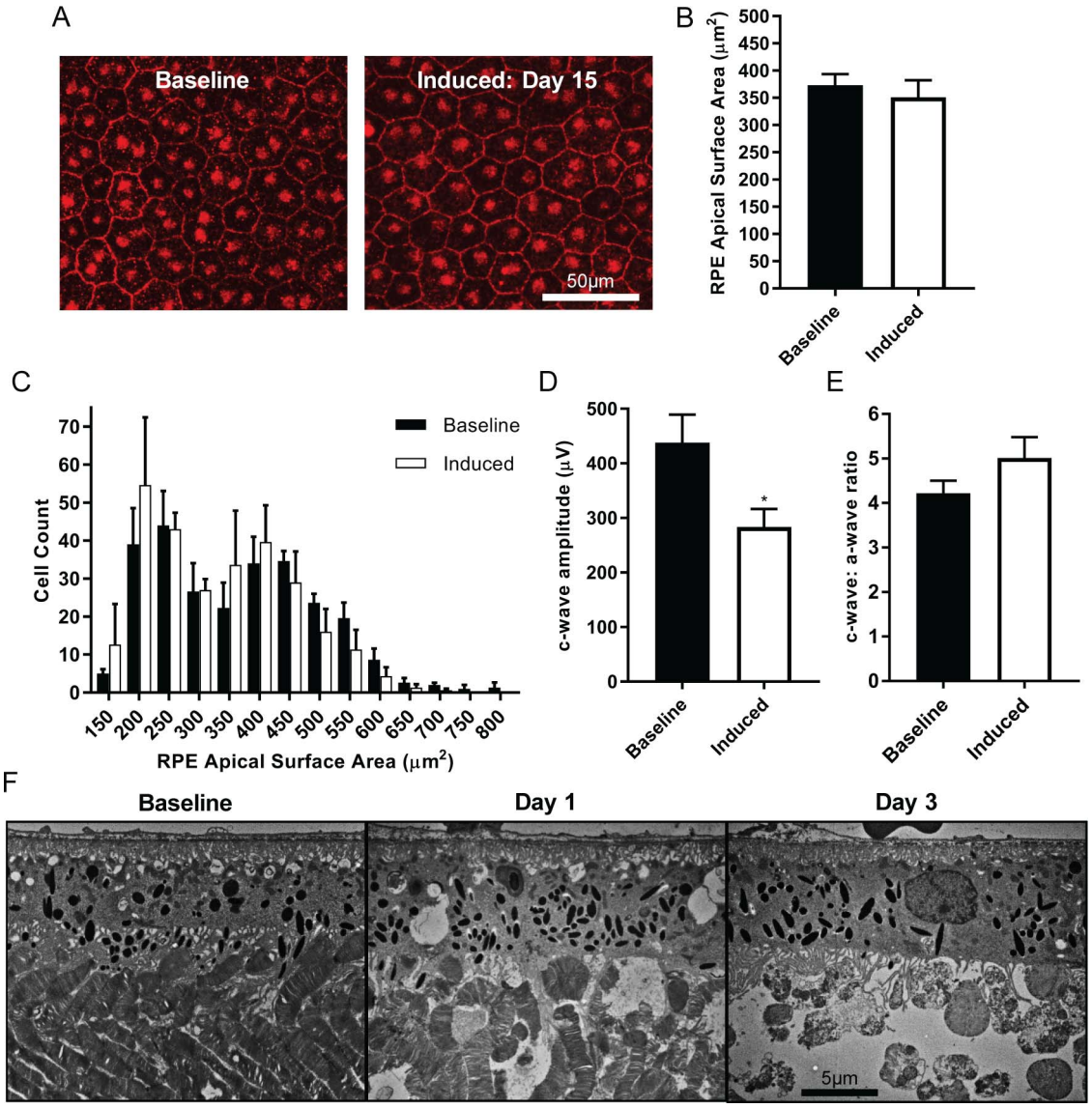

Figure 6. The RPE remains histologically and functionally intact after light damage. (**A–E**) I307N *Rho* mice were either exposed to ambient light or subjected to 20,000 lux of light for 30 minutes and their RPE was assayed 15 days thereafter. (**A**) The RPE was isolated and stained for the ZO-1 protein (*red*) to visualize the border of individual RPE cells. Displayed are representative visual fields with an original magnification of 40×. (**B**) The apical surface area of approximately 240 RPE cells in individual mice was measured in $n = 3$ mice per group. The bar graph represents the mean RPE apical surface area in $\mu m^2 \pm$ SEM. (**C**) A histogram with 50 μm^2 wide bins centered on the surface area values on the X-axis was generated to analyze the spectrum and distribution of RPE apical surface areas. The graph represents the mean number of RPE cells that achieved a particular apical surface area in a sample of $n = 3$ mice per group. Error bars show the SEM. (**D**) The c-wave amplitude of the scotopic ERG waveform was significantly decreased in the induced compared to baseline I307N *Rho* mouse. (**E**) Maintenance of the c-wave to a-wave ratio in the induced animal suggested that the diminution of the c-wave occurred due to relative photoreceptor inactivity rather than the RPE injury. (**F**) Electron microscopy images with an original magnification of 5000× to visualize the RPE. Disordered outer segments were evident 1 day after light challenge, which were noticeably cleared by day 3.

the cell border of RPE cells.[34] We subsequently measured the two-dimensional apical surface area of individual RPE cells (Fig. 6A). The average surface area across a population of RPE cells was slightly smaller in I307N *Rho* mice that had been exposed to light 15 days beforehand compared to naïve I307N *Rho* mice (Fig. 6B). We next analyzed the spectrum and distribution of apical surface areas of individual RPE cells by generating histograms. Both treatment groups displayed similar bimodal distributions, with most RPE cells achieving a surface area between 200 and 550 μm^2 (Fig. 6C).

We subsequently examined the functional capacity of the RPE in vivo after light injury by measuring the c-wave amplitude of the visual response via ERG (Fig. 6D, 6E). A significant decrease in the c-wave amplitude was detected in I307N *Rho* mice that had been exposed to 30 minutes of 20,000 lux of light 15 days beforehand compared to naïve littermates (Fig. 6D). However, the c-wave has been proposed to represent the absorption of extracellular K^+ by the RPE that was released from photoreceptors during phototransduction.[35] Therefore, diminution of the c-wave may reflect a reduction in photoreceptor activity, rather than injury to the RPE. Indeed, the c- to a-wave ratio was not significantly different between induced and naïve I307N *Rho* mice (Fig. 6E).

Finally, substantial clearance of the residual photoreceptor outer segments occurred between days 1 and 3 following light challenge, which suggests that the RPE is only transiently

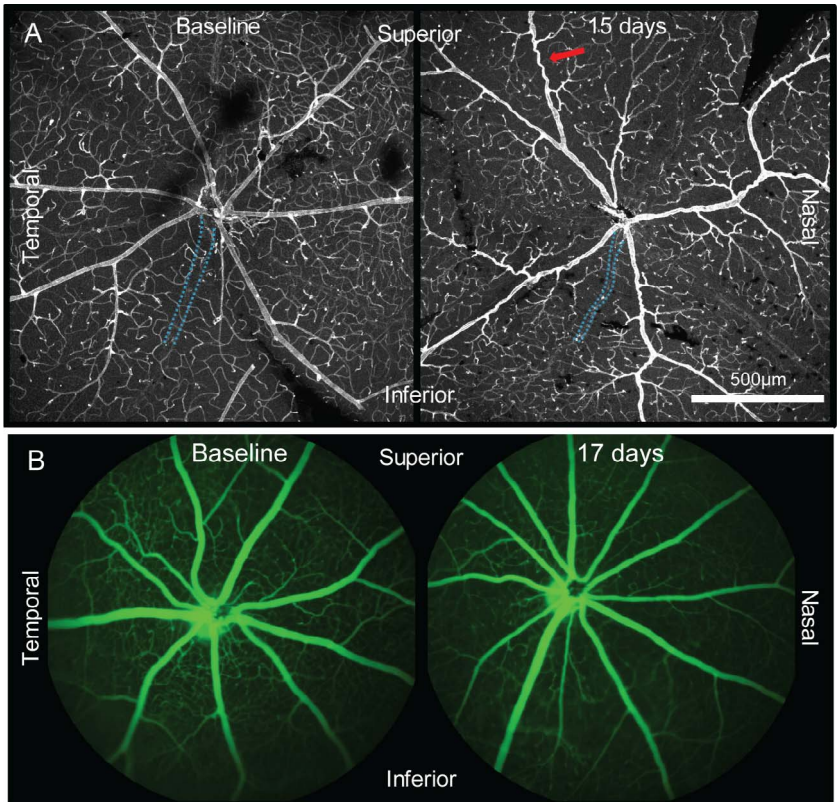

Figure 7. Atrophy of the major vessels of the retina occurs with light-induced degeneration of the I307N *Rho* mouse. I307N *Rho* mice received only ambient light exposure or were challenged with 20,000 lux of light for 30 minutes. (**A**) Fifteen days thereafter, mice were euthanized to prepare retinal wholemounts stained with GSL IB4 (*white*, $n = 3$ per group). Atrophy of the large retinal vessels was apparent in the animals exposed to bright light (*right panel*) compared to those that did not receive a light challenge (*left panel*). Arteries appeared tortuous (*red arrow*) and veins were relatively collapsed (*blue outlines*), especially in the inferior retina, after light challenge. (**B**) Fluorescence angiography was performed with the Micron III fundus microscope to assess the retinal vasculature in the living animal before (*left panel*) or 17 days after (*right panel*) light damage ($n = 2$ per group).

exposed to potentially damaging substances derived from dying photoreceptors. While we observed some increases in membrane-containing vacuoles in the RPE on day 1 following light injury, by day 3, the ultrastructure of the RPE was normal (Fig. 6F). This observation indicated that the RPE is capable of removing substantial biomass, likely with the help of microglia, from the subretinal space during photoreceptor cell death in the I307N *Rho* mouse. Taken together, atrophy of the RPE does not appear to be a feature of retinal degeneration in the I307N *Rho* mouse.

Atrophy of the Major Retinal Vessels

The initial characterization of the I307N *Rho* mouse reported pigmentation in the fundus, an important sign of RP on clinical examination.[1,5] Since attenuated blood vessels constitute another classic finding of RP in humans, we hypothesized that changes to the major retinal vessels would occur following light challenge. We therefore isolated retinas from I307N *Rho* mice before or 15 days after light damage to prepare retinal whole mounts stained with *Griffonia simplicifolia* lectin I isolectin B4 (GSL IB4), which binds glycoproteins of endothelial cells (Fig. 7A). The major vessels that emanated from the ONH in the light-exposed retinas appeared more collapsed when compared to the baseline sample. Furthermore, tortuous segments of arteries that were absent at baseline were apparent in the light-challenged mice.

To ensure that the unhealthy patterning of the vasculature detected via whole mount was not an artifact of tissue preparation postmortem, fluorescence angiography of the fundus was performed on animals before and 20 days after light damage (Fig. 7B). Though the tortuous nature of the vasculature was not as obvious, the major retinal vessels appeared to be smaller in diameter. Moreover, the capillaries that supplied the retina appeared sparser or less perfused. Therefore, similar to patients afflicted with RP, light-exposed I307N *Rho* mouse exhibited attenuation of the major vessels of the retina.[36]

Discussion

The I307N *Rho* mouse shares important clinical signs of RP with the human form of the disease, which include impaired dark adaptation, retinal pigmentation, rod and cone photoreceptor loss, glial activation, and vascular anomalies on the fundus exam, the last of which is described here.[5,6,36] We and others have shown that retinal degeneration in the I307N *Rho* mouse is inducible and tunable.[5,6] In this regard, we observed that extending the duration of exposure of 20,000 lux of light from 10 to 30 minutes increased the magnitude and area of ONL loss.

Of note, our light damage protocol was significantly different from those utilized by the other two studies that induced retinal degeneration in I307N *Rho* mice with light

cages equipped with mirrored walls[5,6]; our cages, however, emitted light only from the roof.[22] The position of the light relative to the mouse may determine the area of the retina that receives illumination and thus the extent of retinal degeneration. Because the source and intensity of illumination as well as the duration of exposure can be varied, the extent of damage can be titrated to fit the needs of a particular experiment. In this way, the I307N *Rho* mouse presents an opportunity to explore either mild/focal or severe/widespread retinal degeneration. We also found that the I307N *Rho* mouse differs from other RP mouse models in that the injury to the ONL is not progressive, and partial ONL loss can be achieved with lower exposure times (e.g., 10 minutes). Resolution of photoreceptor injury can therefore be dissected in the I307N *Rho* mouse.

An important consideration when designing a light damage protocol for the I307N *Rho* mouse is that retinal damage may be easier to detect in the setting of a histological sample compared to SD-OCT. We observed that the focus of injury occurred in the inferonasal quadrant of a 1.4 mm by 1.4 mm window of the retina centered on the ONH. Because we image only the central posterior retina and illumination came from above, more intense and long-lasting exposures to light were necessary to achieve a detectable phenotype by SD-OCT within this central window. Subtler and more eccentric retinal damage may require imaging of multiple windows and subsequent montaging for detection. We also observed that our continued backcrossing of the I307N *Rho* mouse to the C57BL/6 strain conferred resistance to light damage. The presence of disease-modifying genes or differences in pigmentation may affect the sensitivity of the I307N *Rho* mouse to light[37,38]; thus, different I307N *Rho* colonies may require longer or more intense exposures to light. As with other strains on the B6 background, our colony expressed the hypomorphic Leu450Met variant of RPE65.

In performing efficacy studies utilizing the I307N *Rho* mouse, clinically-relevant endpoints should be employed to establish a therapeutic effect and to permit comparison with human RP. ERG and SD-OCT have become cornerstones of efficacy studies in mouse and human since repeated measurements can be performed over time and with minimal risk of injury to the retina.[19] Our SD-OCT analysis thus has important implications for future efficacy studies. In particular, we demonstrated that retinal degeneration induced in the I307N *Rho* mouse by an overhead light was more severe in the inferior and nasal retinal quadrants compared to the temporal and superior retinal quadrants. The protective effects of a therapy could be explored in the setting of total ONL loss in the inferonasal retina or partial ONL loss in the superotemporal retina of the same eye. Our results also indicate that therapeutic endpoints involving SD-OCT can be terminated as early as 1 week after light injury because differences in ONL thickness were minimal thereafter. Furthermore, we corroborated the findings by Gargini et al.[6] that deterioration of the ERG response can be detected by day fifteen after light challenge, and also demonstrated that the c-wave decreased with loss of photoreceptor activity rather than RPE injury. We recommend performing ERG at least 2 weeks following light challenge because acute inflammatory processes can inhibit phototransduction and the visual response.[39] Finally, our data suggested that pathologic alterations to the vasculature of the I307N *Rho* mouse can be explored 15 days after light injury, and even as early as day 8 (unpublished data, 2018).

The mechanisms leading to rod photoreceptor loss in the I307N *Rho* mouse remain poorly understood. Budzynski et al.[5] proposed that constitutive activation of the phototransduction cascade underlies retinal degeneration in the I307N *Rho* mouse. Indeed, they found that the I307N $Rho^{+/-}$ / $rd12^{+/+}$ mouse, which lacks all-*trans*-retinoid isomerase activity, experienced retinal degeneration in the absence of bright light.[5,40] Nonetheless, whether constitutive activation of the phototransduction cascade contributes to retinal degeneration in the I307N *Rho* mouse would be more accurately explored by generating I307N $Rho^{+/-}$ / $GNAT1^{-/-}$ mice and subsequently challenging them with bright light.[24,41]

The most striking SD-OCT features that we observed in the I307N *Rho* mouse were tissue swelling 1 day after light challenge, and generation of hyper-reflective signal that appeared between the OPL and subretinal space. These aspects are common among light-sensitive retinal degeneration mouse models, especially the $arrestin^{-/-}$ mouse.[24,42] A hyper-reflective ONL has also been observed in animal models of light-independent retinal degeneration, including the *rd1* and *rd10* mice as well as Royal College of Surgeons' rats.[43,44] Our data suggested that SD-OCT hyper-reflectivity correlates with ONL loss, as both predominate in the inferonasal retina. Therefore, identifying the sequential events that lead to the hyper-reflective signal may enhance our understanding of the poorly understood retinal degeneration in the I307N *Rho* mouse, and RP in general.

We have observed that the hyper-reflectivity of the OPL appears before obvious retinal swelling and subretinal hyper-reflectivity (unpublished data, 2018). The reflective signal may coincide with the onset of influx of fluid that generates retinal swelling on day 1.[27] Others have reported that leakiness of the inner retinal vasculature[42] and RPE[45] occurs in the setting of light injury. Reactive Müller glia may also redistribute fluid to the outer retina by altering their expression of aquaporin-4 and the Kir4.1 potassium channel after light-injury.[46] Intriguingly, the early obliteration of the OLM and disconnect of photoreceptor nuclei from their inner and outer segments could modify the fluid balance of the retina, as the inner retina and subretinal space, which are normally compartmentalized, can now communicate. These latter events are evident in the light-sensitive $arrestin^{-/-}$ mouse and may produce the hyper-reflectivity of the subretinal space.[24]

Hyper-reflective signals might indicate the onset of photoreceptor apoptosis in the I307N *Rho* mouse.[5,24,29,30] Similar to the $arrestin^{-/-}$ mouse after light exposure,[24] we observed that the chromatin within the photoreceptor nuclei condensed during the period of hyper-reflectivity, and condensed chromatin may present a barrier to the passage of infrared light during SD-OCT. Furthermore, retention of ECM or membranes around nuclei-free space in the ONL of the I307N *Rho* mouse during the acute phase after light damage could produce a new solid/liquid interface and a refractive transition that generates abundant reflective events. Of note, these photoreceptor cell ghosts were near the borders of the ONL with the OPL and subretinal space, which are the apparent sources of the hyper-reflective signal. Additionally, the disappearance of photoreceptor nuclei implies phagocytic activity of microglia in the ONL, which has been previously reported in the I307N *Rho* mouse.[6] We have also observed profound morphological changes, expansion, and migration of microglia to the ONL that could present an obstacle to the passage of light during SD-OCT or disrupt the tight packing of photoreceptor cell bodies (unpublished data, 2018).

Our study presents the first SD-OCT characterization of the pattern of light-induced degeneration in the I307N *Rho* mouse. Since SD-OCT is used clinically to document retinal degeneration, our results permit comparison of inherited retinal degeneration in the I307N *Rho* mouse and human using this technology. More specifically, our data provide a thorough timeline of detectable changes on SD-OCT that can be utilized to designate appropriate time points for preclinical efficacy studies and mechanistic studies for future experimentation. Determining the sequential causes of the hyper-reflective

signal on SD-OCT may provide important information regarding RP pathogenesis.

Materials and Methods

Animal Models

The experiments adhered to the ARVO Statement for the Use of Animals in Ophthalmic and Vision Research. All procedures received prior approval from the Institutional Animal Care and Use Committee at the University of Florida. The I307N *Rho* (Tvrm4) mouse line was a kind gift of Patsy Nishina, PhD,[5] and were bred to the Jackson Laboratory C57BL/6 strain (The Jackson Laboratory, Bar Harbor, ME, USA) for at least eight generations. Experimental and breeder mice were housed in an Animal Care Services accredited facility in a room with a 12:12-h dim-red light:dark lighting cycle. The intensity of the dim red light was less than 200 lux. Genotyping was performed with the REDExtract-N-AMP Tissue PCR Kit as per the manufacturer's instructions (Sigma-Aldrich Corp., St. Louis, MO, USA). The PCR reaction was performed with an annealing temperature of 61°C with the following oligonucleotides (Forward: GGTCATCTTCTTCCTGATCTGCTGGC, Reverse: TGCCAG CAGTCTGAGTGCAATG). The PCR product is a 259 base-pair genomic region that contains the I307N mutation, which introduces an *AflIII* restriction site. The I307N *Rho* PCR-fragment, when incubated with AflIII (New England Biolabs, Ipswich, MA, USA), liberates two fragments of approximately 150 and 110 base-pairs. The WT *Rho* PCR-fragment retina retains the full 260 base-pair length. Homozygous I307N *Rho* mice were employed as breeders and heterozygous I307N Rho mice were employed for experimentation.

Induction of Light Damage

Strips of LED lights (DC24V, LEDmy, Shenzhen Futian District, CHN) were adhered to the underside of standard cage lids (Supplementary Fig. S1A). The wires leading to the LED lights were spliced with an adapter such that the desktop AC adapter 90W 24V 3.75A (GS90A24-P1M, Mean Well, New Taipei City, Taiwan) could function as the power source. A LED dimmer was attached in series between the LED lights and power supply to modulate the light intensity. Light intensity within the cage was measured with a dual-range traceable light meter (Control Company, Webster, TX, USA) placed on the floor of the cage. Light intensity was set to 20,000 lux with the dimmer.

Mice aged 8 to 12 weeks old were dark adapted for greater than 4 hours. The light damage protocol was initiated between the hours of 10:00 PM and 12:00 AM such that the light damage was completed no later than 1:00 AM. The pupils of mice to be light damaged were dilated by application of 1% atropine (Akorn, Lake Forest, IL, USA) and 2.5% phenylephrine (Paragon BioTeck, Inc., Portland, OR, USA) eye drops followed by a 15-minute waiting period, a second application of phenylephrine followed by a second 15-minute waiting period, and a third application of phenylephrine just prior to placing the mice in the light cages (Supplementary Fig. S1B). Once in the cage, the power supply to the LED cage lids was initiated to provide a 20,000 lux light intensity to the floor of the cage. Mice were allowed to walk freely in the lit cage for 10, 20, or 30 minutes and displayed no aversion to the light. Once the light damage period was completed, the mice were returned to their housing cage and quickly returned to the room with a 12:12-h dim-red light:dark lighting cycle.

Spectral-Domain Optical Coherence Tomography (SD-OCT)

Mice were anesthetized via intraperitoneal injection with a cocktail of 4 mg/kg xylazine (Vedco, St. Joseph, MO, USA) and 100 mg/kg ketamine (Vedco). At the time of anesthesia injection, the pupils of the mice were dilated with 2.5% phenylephrine eye drops (Paragon BioTeck, Inc.). The Envisu SD-OCT ophthalmic imaging system was used to capture 25 B-scans across the retina, each representing the average of 10 frames–250 total frames (Leica Microsystems, Durham, NC, USA). The 25 B-scans covered an area of 1.4 mm × 1.4 mm of retina. ONL thickness was measured in each of the SD-OCT scans utilizing calipers in the Bioptigen Diver software (Leica Microsystems, Durham, NC, USA). Measurements were performed at specific locations situated −500, −375, −250, 250, 375, and 500 μm along the vertical or horizontal axis with reference to the optic nerve head (ONH). ONL thickness was measured from the interface of the ONL and OPL to the interface of the ONL and OLM. The total retinal thickness was measured as the distance from the interface of the NFL and vitreous chamber to the interface of the RPE and choroid. The INL was measured as the distance from the interface of the INL and OPL to the interface of the INL and IPL. The measurement of the inner retina represented the distance from the interface of the INL and IPL to the interface of the NFL and vitreous chamber.

Data were prepared for bar graphs by averaging the six measurements taken within a quadrant of the right and left eye of a single eye (e.g., the 250, 375, and 500 μm positions superior to the ONH in both the right and left eye) to obtain an averaged quadrant measurement. Bar graphs were generated and 1-way (Fig. 1) or 2-way ANOVA (Fig. 2; Supplementary Fig. S3) followed by multiple comparisons tests were performed with GraphPad Prism 5 software (GraphPad Software, San Diego, CA, USA). Multiple Student's *t*-tests were also employed when appropriate (Fig. 5).

Area of the Subretinal Detachment

The area of the subretinal detachment was measured with ImageJ (https://imagej.nih.gov/ij/). SD-OCT B scans that were centered on the ONH were loaded in ImageJ and the color was inverted to increase the contrast of the subretinal detachment. The scale of the image was set such that 1024 pixels equaled 1400 μm. A polygon was drawn around the subretinal detachment in the nasal retina within a 650 μm segment of the retina that began at the ONH (Fig. 5D). The subretinal detachment was measured as the area of the drawn polygon. A bar graph was generated to describe the data and an unpaired two-tailed Student's *t*-test was performed with Prism 5 software (GraphPad Software).

Electroretinography (ERG)

Scotopic simultaneous, full-field ERG was performed as previously described.[14] Mice were dark adapted for greater than 4 hours and their pupils were dilated with one application of 1% atropine (Akorn, Lake Forest, IL, USA) and 2.5% phenylephrine eye drops (Paragon BioTeck, Inc.) 15 minutes prior to visual testing. Mice were anesthetized with a cocktail of xylazine and ketamine. Upon loss of consciousness, GenTeal Tears lubricant eye gel (Alcon, Fort Worth, TX, USA) was applied to the surface of each cornea to inhibit drying and to ensure a strong current. For scotopic ERG, mice were immediately placed in the UTAS Big Shot Ganzfield Illuminator (LKC Technologies, Gaithersburg, MD, USA) and wire-loop electrodes were positioned on the corneal surface. A single

Investigative Ophthalmology & Visual Science

reference electrode was inserted subcutaneously between the ears, and a single ground electrode was placed subcutaneously near the tail. The electrical activity of the retina was recorded with a UTAS-E 2000 Visual Electrodiagnostic System (LKC Technologies, Gaithersburg, MD, USA) in response to a program of brief flashes of white light with intensities of: 0 dB = 2.5 cd·sec/m^2, −10 dB = 0.25 cd·sec/m^2, and −20 dB = 0.025 cd·sec/m^2. The electrical response was measured as the average response to five individual flashes of each light intensity separated in time. In the case of the −20 dB and −10 dB conditions, a 5-second rest period separated each light flash, whereas a longer 60-second rest period was used for the 0dB intensity. The a-wave and b-wave amplitudes from the averaged electrical response for each flash intensity were calculated using a custom Excel program that identified the maximum negative deflection (a-wave) and maximum positive deflection (b-wave) of the electrical signal over time.

ERG for the c-wave and b-wave to a-wave ratio was performed as previously described with the Espion full-field ERG system[47] (Diagnosys Systems, Westford, MA, USA). Mice were prepared the same as for scotopic ERG except the reference and ground electrodes were placed in the cheek and tail, respectively. The retina was stimulated with flashes of white light with an intensity of 2.7 cd·sec/m^2. The c-wave was measured as the maximum value of the electrical response curve between 1 and 4 seconds after the light flash minus the baseline value of the curve.

The data were prepared for bar graphs by averaging the a-wave, b-wave, or c-waves amplitudes of the right and left eyes of individual mice. Bar graphs were generated and 1-way ANOVA followed by multiple comparisons tests for flash intensities individually (Supplementary Fig. S2A, S2B) or unpaired Student's *t*-tests (Supplementary Fig. S2C; Fig. 6D, 6E) were performed with GraphPad Prism 5 (GraphPad Software).

Longitudinal Reflectivity Profiles and Area Under the Curve

The OCT B-scan, centered on the ONH for an individual eye, was loaded in the ImageJ software (https://imagej.nih.gov/ij/). The image was converted to an 8-bit grayscale format, then the color was inverted. The scale of the image was set such that 1024 pixels equaled 1400 μm. A rectangle with a height of 50 μm and width of 750 μm (the spacing box) was drawn so that its center was positioned over the ONH and its lower corners made tangential contact with the interface between the NFL and the vitreous chamber. The B-scan was rotated until the retina was horizontal. A second rectangle with a height of 450 μm and width of 20 μm (the measurement box) was positioned in the nasal portion of the B-scan at the same height as, but just lateral to, the centered 750 μm rectangle (Supplementary Fig. S5A). The reflectivity profile within the measurement boxes was generated with the analyze gel function, first by establishing the box as the first gel lane (Ctrl + 1) then by selecting plot lanes (Ctrl + 3; Supplementary Fig. S5B). The resulting plot was transformed vertically and then saved as *X*–*Y* coordinates. This sequence was repeated to measure the reflectivity of the temporal retina, except placing the measurement box in the temporal portion of the retina. The *X*–*Y* coordinates were loaded into Excel and missing *X*-values were inserted using a simple Excel program (https://www.youtube.com/watch?v=zktCVGfH1_k; Supplementary Fig. S5C–E). The *X*-values, which represent the distance in pixels of the gel plot, were transformed to μms (450 μm / 650 pixels).

The reflectivity plot data were prepared for graphical representation by averaging the *Y*-values of corresponding *X*-values for the nasal or temporal portion of the right and left eye of individual mice. Averaged reflectivity plots were then input into GraphPad Prism 5 (GraphPad Software) as an *X*–*Y* scatter plot with a connecting line. Since the procedure is reproducible between mice, averaged reflectivity plots from separate mice could be inserted as replicates to produce a plot representing the mean and SEM of reflectivity at a given time point.

To measure the area under the curve of the area of inversion, vertically transformed gel plots (Supplementary Fig. S5B) were loaded in the ImageJ software. A box with a size equal to the height of the plot and a width of 160 pixels was positioned to span between the INL and the middle of the subretinal space. The wand tool was used to select and measure the AUC. Of note, the AUC is the area over the curve in the vertically transformed gel plot. The data were prepared for bar graphs by averaging the AUC values for the nasal or temporal retina of the right and left eye of an individual mouse. Bar graphs were generated and 2-way ANOVA were performed, followed by multiple comparisons tests with GraphPad Prism 5 (GraphPad Software).

Plastic Sections, Light Microscopy, and Electron Microscopy

Samples were prepared as previously described.[48] Mice were overdosed with sodium phenobarbital then perfused systemically with 4% paraformaldehyde and 2% glutaraldehyde in phosphate buffered saline (PBS). Eyes were removed from the animal and incubated with fresh 4% paraformaldehyde and 2% glutaraldehyde in PBS overnight at 4°C. The tissue was washed with 0.1 M cacodylate (pH7.4) before incubation with 1% osmium tetroxide for 4 hours at 4°C. The tissue was then washed overnight with 0.1 M cacodylate (pH 7.4) at 4°C. Samples were dehydrated with successive washes with increasing concentrations of ethanol up to 100% and then rotated in epoxy/propylene for embedding. Sections of 80–100 nm or 1-μm thick were prepared for electron microscopy with the SU5000 Schottky Field-Emission microscopy (Hitachi, Tokyo, Japan) and light microscopy with the Biorevo BZ-9000 microscope (Keyence, Osaka, Japan).

Immunohistochemistry of PFA-Fixed Frozen Sections

Mice were euthanized via CO_2 inhalation and cervical dislocation. Eyes were gently excised and briefly washed in PBS before incubation in paraformaldehyde (PFA; Electron Microscopy Sciences, Hatfield, PA, USA) diluted to 4% in PBS for 5 minutes at room temperature. The cornea was then excised, and the lens was removed before the eye was incubated in 4% PFA for an additional 20 minutes at room temperature. Eyes were then placed in 30% sucrose and stored at 4°C for 48 hours for cryoprotection. Eyes were frozen with the vapors of liquid nitrogen in Optimal Cutting Temperature Compound (Sakura, Torrance, CA, USA) in a histology disposable base mold (Electron Microscopy Sciences). 16-μm sections were obtained with the Leica CM3050 S cryostat (Leica, Wetzlar, Germany). To stain, slides were assembled on the Shandon Sequenza slide rack (Fisher Scientific, Hampton, NH, USA). Tissue sections were hydrated with PBS, permeabilized with PBS containing 0.5% Triton X-100 (PBS-T; Fisher Scientific), incubated with 0.5% sodium borohydride (Sigma-Aldrich Corp.) in PBS, washed with PBS, and blocked with 10% normal horse serum (Vector Laboratories) in PBS-T (blocking buffer) for 1 hour at room temperature. Anti-synaptophysin (Millipore, Burlington, MA, USA) diluted to 1:300 in blocking buffer was incubated on the

Investigative Ophthalmology & Visual Science

tissue at 4°C overnight. The primary antibody solution was removed with PBS-T washes before incubation with donkey anti-mouse IgG (H+L) secondary antibody (Fisher Scientific) diluted to 1:2000 in blocking buffer for 1 hour at room temperature. PBS washes were performed before DAPI (D1306; Thermo Fisher) diluted to 1:7000 in PBS was applied to the tissue for 10 minutes. Slides were coverslipped using Fluoromount-G (Thermo Fisher) and imaged using the DMi8 confocal microscope (Leica).

Immunohistochemistry of RPE Wholemounts

Mice were euthanized by CO_2 inhalation and cervical dislocation. Eyes were marked with green animal tattoo ink (Ketchum Manufacturing Co., Lake Luzerne, NY, USA) at the nasal margin of the cornea then excised with curved forceps. Eyes were incubated in paraformaldehyde (PFA) (Electron Microscopy Sciences) diluted to 1% in PBS for 1 hour on ice. The cornea was removed, and a small cut was made on the nasal margin of the cornea to maintain orientation throughout the staining procedure. The retina was gently separated from the RPE by cutting the ONH before a second incubation in PFA diluted to 4% in PBS for 20 minutes at room temperature.

The retina and RPE were washed and permeabilized in PBS-T for 30 minutes at room temperature on an orbital shaker. The retina, but not RPE, was incubated with 0.5% sodium borohydride (Sigma-Aldrich Corp.) for 30 minutes at room temperature then washed in PBS for >10 minutes. Retinal and RPE tissue were blocked with 10% normal horse serum (Vector Laboratories) in PBS-T blocking buffer overnight at 4°C. Biotinylated *Griffonia simplicifolia* lectin I isolectin B4 (GSL IB4; Vector Laboratories) diluted to 1:500 in blocking buffer was incubated with retinal tissue for 3 days at 4°C, whereas anti-ZO-1 (Invitrogen, Carlsbad, CA, USA) diluted to 1:200 was incubated with RPE tissue overnight at 4°C. Tissues were subsequently washed with PBS-T. Streptavidin, Alexa Fluor 594 conjugate (Thermo Fisher) diluted to 1:500 in blocking buffer was applied to the retinal tissue and incubated for 2 hours at room temperature. Donkey anti-rabbit IgG (H+L) secondary antibody, Alexa Fluor 594 (Thermo Fisher), diluted to 1:1000 in blocking buffer, was applied to RPE tissue and incubated for 1 hour at room temperature. Tissue was washed, dissected to a clover leaf configuration, coverslipped using Fluoromount-G (Thermo Fisher), and imaged using the DMi8 confocal microscope (Leica).

Measurement of RPE Apical Surface Area

Images of a 290 μm by 290 μm area of the RPE wholemount (40× original magnification) were loaded in ImageJ (https://imagej.nih.gov/ij/) and the scale was set accordingly. Four non-overlapping 150-μm by 150-μm boxes were drawn toward each corner of the image. The apical surface area of individual RPE cells that either lied within or crossed the border of the box was measured by drawing a polygon around each cell and measuring its area. We believed that excluding RPE cells that crossed the border of the box would disproportionately exclude the larger RPE cells from analysis. The surface area of approximately 120 RPE cells was typically measured in each image. Additionally, two individual 40× images were analyzed per mouse, which increased the total number of surveyed RPE cells to approximately 240 per mouse. A bar graph of the average RPE area was generated and a non-paired 2-tailed Student's *t*-test was performed with GraphPad Prism 5 (GraphPad Software). Matlab (MathWorks, Natick, MA, USA) was utilized to generate the data for histograms, whereas GraphPad Prism 5 (GraphPad Software) was employed to create the histogram graph and to perform statistical analyses.

Fluorescence Angiography

The pupils of mice were dilated by application of 1% atropine (Akorn) and 2.5% phenylephrine eye drops (Paragon BioTeck, Inc.). Mice were then injected with 20 μL of 10% fluorescein (AK-FLUOR; Akorn) into their intraperitoneal cavity. After 15 minutes, mice were anesthetized with a cocktail of xylazine and ketamine (Vedco). Upon loss of consciousness, a scout SD-OCT was performed (described previously) to ensure that light damage was successful. Mice were immediately placed on a mobile stage, GONAK 2.5% hypromellose solution (Akorn) was applied to the corneal surface, and green fluorescent fundus images were captured utilizing the Micron III fundus camera (Phoenix Research Labs, Pleasanton, CA, USA). The images were captured between 20 and 25 minutes after injection of the fluorescein.

Acknowledgments

The authors thank John Ash, PhD, Casey Keuthan, and Clayton Santiago, PhD, for pointing out the utility of the illumination cages and for making his cages available to us.

Supported by Training Grant F30EY027163 (awarded to MTM), by a NEI Core Grant to the University of Florida (P30 EY02172), and by the Shaler Richardson Professorship Endowment (ASL).

Disclosure: **M.T. Massengill**, None; **B. Young**, None; **D. Patel**, None; **F. Jafri**, None; **E. Sabogal**, None; **N. Ash**, None; **H. Li**, None; **C.J. Ildefonso**, None; **A.S. Lewin**, None

References

1. Verbakel SK, van Huet RAC, Boon CJF, et al. Non-syndromic retinitis pigmentosa. *Prog Retin Eye Res*. 2018;66:157–186.
2. Rossmiller B, Mao H, Lewin AS. Gene therapy in animal models of autosomal dominant retinitis pigmentosa. *Mol Vis*. 2012;18:2479–2496.
3. Daiger SP, Sullivan LS, Bowne SJ. RetNet: Summaries of Genes and Loci Causing Retinal Diseases: University of Texas-Houston Health Science Center; 2018. Available at: http://www.sph.uth.tmc.edu/RetNet/. Accessed May 30, 2018.
4. Givre S, Garg S. Retinitis Pigmentosa: Clinical Presentation and Diagnosis; 2018. Available at: https://www.uptodate.com/contents/retinitis-pigmentosa-clinical-presentation-and-diagnosis. Accessed May 30, 2018.
5. Budzynski E, Gross AK, McAlear SD, et al. Mutations of the opsin gene (Y102H and I307N) lead to light-induced degeneration of photoreceptors and constitutive activation of phototransduction in mice. *J Biol Chem*. 2010;285:14521–14533.
6. Gargini C, Novelli E, Piano I, Biagioni M, Strettoi E. Pattern of retinal morphological and functional decay in a light-inducible, rhodopsin mutant mouse. *Sci Rep*. 2017;7:5730.
7. Cideciyan AV, Hood DC, Huang Y, et al. Disease sequence from mutant rhodopsin allele to rod and cone photoreceptor degeneration in man. *Proc Natl Acad Sci U S A*. 1998;95:7103–7108.
8. Xiong W, MacColl Garfinkel AE, Li Y, Benowitz LI, Cepko CL. NRF2 promotes neuronal survival in neurodegeneration and acute nerve damage. *J Clin Invest*. 2015;125:1433–1445.
9. White DA, Fritz JJ, Hauswirth WW, Kaushal S, Lewin AS. Increased sensitivity to light-induced damage in a mouse model of autosomal dominant retinal disease. *Invest Ophthalmol Vis Sci*. 2007;48:1942–1951.

10. Dutta S, Sengupta P. Men and mice: relating their ages. *Life Sci*. 2016;152:244–248.
11. Kim JW, Yang HJ, Brooks MJ, et al. NRL-regulated transcriptome dynamics of developing rod photoreceptors. *Cell Rep*. 2016;17:2460–2473.
12. Olsson JE, Gordon JW, Pawlyk BS, et al. Transgenic mice with a rhodopsin mutation (Pro23His): a mouse model of autosomal dominant retinitis pigmentosa. *Neuron*. 1992;9: 815–830.
13. Kong F, Li W, Li X, et al. Self-complementary AAV5 vector facilitates quicker transgene expression in photoreceptor and retinal pigment epithelial cells of normal mouse. *Exp Eye Res*. 2010;90:546–554.
14. Mao H, Gorbatyuk MS, Rossmiller B, Hauswirth WW, Lewin AS. Long-term rescue of retinal structure and function by rhodopsin RNA replacement with a single adeno-associated viral vector in P23H RHO transgenic mice. *Hum Gene Ther*. 2012;23:356–366.
15. Sakami S, Maeda T, Bereta G, et al. Probing mechanisms of photoreceptor degeneration in a new mouse model of the common form of autosomal dominant retinitis pigmentosa due to P23H opsin mutations. *J Biol Chem*. 2011;286:10551–10567.
16. Mao H, James T, Schwein A, et al. AAV delivery of wild-type rhodopsin preserves retinal function in a mouse model of autosomal dominant retinitis pigmentosa. *Hum Gene Ther*. 2011;22:567–575.
17. Aleman TS, Cideciyan AV, Sumaroka A, et al. Retinal laminar architecture in human retinitis pigmentosa caused by Rhodopsin gene mutations. *Invest Ophthalmol Vis Sci*. 2008;49:1580–1590.
18. Jacobson SG, Matsui R, Sumaroka A, Cideciyan AV. Retinal structure measurements as inclusion criteria for stem cell-based therapies of retinal degenerations. *Invest Ophthalmol Vis Sci*. 2016;57:ORSFn1–ORSFn9.
19. Adhi M, Duker JS. Optical coherence tomography – current and future applications. *Curr Opin Ophthalmol*. 2013;24: 213–221.
20. Berger A, Cavallero S, Dominguez E, et al. Spectral-domain optical coherence tomography of the rodent eye: highlighting layers of the outer retina using signal averaging and comparison with histology. *PLoS One*. 2014;9:e96494.
21. Arango-Gonzalez B, Schatz A, Bolz S, et al. Effects of combined ketamine/xylazine anesthesia on light induced retinal degeneration in rats. *PLoS One*. 2012;7:e35687.
22. Ueki Y, Wang J, Chollangi S, Ash JD. STAT3 activation in photoreceptors by leukemia inhibitory factor is associated with protection from light damage. *J Neurochem*. 2008;105: 784–796.
23. Downs LM, Scott EM, Cideciyan AV, et al. Overlap of abnormal photoreceptor development and progressive degeneration in Leber congenital amaurosis caused by NPHP5 mutation. *Hum Mol Genet*. 2016;25:4211–4226.
24. Levine ES, Zam A, Zhang P, et al. Rapid light-induced activation of retinal microglia in mice lacking Arrestin-1. *Vision Res*. 2014;102:71–79.
25. Li Y, Zhang Y, Chen S, Vernon G, Wong WT, Qian H. Light-dependent OCT structure changes in photoreceptor degenerative rd10 mouse retina. *Invest Ophthalmol Vis Sci*. 2018; 59:1084–1094.
26. Jacobson SG, McGuigan DB, Sumaroka A, et al. Complexity of the class B phenotype in autosomal dominant retinitis pigmentosa due to rhodopsin mutations. *Invest Ophthalmol Vis Sci*. 2016;57:4847–4858.
27. Labin AM, Safuri SK, Ribak EN, Perlman I. Müller cells separate between wavelengths to improve day vision with minimal effect upon night vision. *Nat Commun*. 2014;5: 4319.
28. Zhao L, Zabel MK, Wang X, et al. Microglial phagocytosis of living photoreceptors contributes to inherited retinal degeneration. *EMBO Mol Med*. 2015;7:1179–1197.
29. Hughes AE, Enright JM, Myers CA, Shen SQ, Corbo JC. Cell type-specific epigenomic analysis reveals a uniquely closed chromatin architecture in mouse rod photoreceptors. *Sci Rep*. 2017;7:43184.
30. Solovei I, Kreysing M, Lanctôt C, et al. Nuclear architecture of rod photoreceptor cells adapts to vision in mammalian evolution. *Cell*. 2009;137:356–368.
31. Krishnamoorthy V, Cherukuri P, Poria D, Goel M, Dagar S, Dhingra NK. Retinal remodeling: concerns, emerging remedies and future prospects. *Front Cell Neurosci*. 2016;10:38.
32. Perlman I. Relationship between the amplitudes of the b wave and the a wave as a useful index for evaluating the electroretinogram. *Br J Ophthalmol*. 1983;67:443–448.
33. Zeng H, Ding M, Chen XX, Lu Q. Microglial NADPH oxidase activation mediates rod cell death in the retinal degeneration in rd mice. *Neuroscience*. 2014;275:54–61.
34. Bailey TA, Kanuga N, Romero IA, Greenwood J, Luthert PJ, Cheetham ME. Oxidative stress affects the junctional integrity of retinal pigment epithelial cells. *Invest Ophthalmol Vis Sci*. 2004;45:675–684.
35. Pinto LH, Invergo B, Shimomura K, Takahashi JS, Troy JB. Interpretation of the mouse electroretinogram. *Doc Ophthalmol*. 2007;115:127–136.
36. Yang YJ, Peng J, Ying D, Peng QH. A brief review on the pathological role of decreased blood flow affected in retinitis pigmentosa. *J Ophthalmol*. 2018;2018:3249064.
37. Kim SR, Fishkin N, Kong J, Nakanishi K, Allikmets R, Sparrow JR. Rpe65 Leu450Met variant is associated with reduced levels of the retinal pigment epithelium lipofuscin fluorophores A2E and iso-A2E. *Proc Natl Acad Sci U S A*. 2004;101: 11668–11672.
38. LaVail MM, Gorrin GM. Protection from light damage by ocular pigmentation: analysis using experimental chimeras and translocation mice. *Exp Eye Res*. 1987;44:877–889.
39. Chucair-Elliott AJ, Elliott MH, Wang J, et al. Leukemia inhibitory factor coordinates the down-regulation of the visual cycle in the retina and retinal-pigmented epithelium. *J Biol Chem*. 2012;287:24092–29102.
40. Pang JJ, Chang B, Hawes NL, et al. Retinal degeneration 12 (rd12): a new, spontaneously arising mouse model for human Leber congenital amaurosis (LCA). *Mol Vis*. 2005;11:152–162.
41. Hao W, Wenzel A, Obin MS, et al. Evidence for two apoptotic pathways in light-induced retinal degeneration. *Nat Genet*. 2002;32:254–260.
42. Geiger P, Barben M, Grimm C, Samardzija M. Blue light-induced retinal lesions, intraretinal vascular leakage and edema formation in the all-cone mouse retina. *Cell Death Dis*. 2015;6:e1985.
43. Pennesi ME, Michaels KV, Magee SS, et al. Long-term characterization of retinal degeneration in rd1 and rd10 mice using spectral domain optical coherence tomography. *Invest Ophthalmol Vis Sci*. 2012;53:4644–4656.
44. Adachi K, Takahashi S, Yamauchi K, Mounai N, Tanabu R, Nakazawa M. Optical coherence tomography of retinal degeneration in Royal College of Surgeons rats and its correlation with morphology and electroretinography. *PLoS One*. 2016;11:e0162835.
45. Cachafeiro M, Bemelmans AP, Samardzija M, et al. Hyperactivation of retina by light in mice leads to photoreceptor cell death mediated by VEGF and retinal pigment epithelium permeability. *Cell Death Dis*. 2013;4:e781.
46. Iandiev I, Pannicke T, Hollborn M, et al. Localization of glial aquaporin-4 and Kir4.1 in the light-injured murine retina. *Neurosci Lett*. 2008;434:317–321.

Investigative Ophthalmology & Visual Science

47. Ildefonso CJ, Jaime H, Brown EE, et al. Targeting the Nrf2 signaling pathway in the retina with a gene-delivered secretable and cell-penetrating peptide. *Invest Ophthalmol Vis Sci*. 2016;57:372–386.

48. Biswal MR, Ahmed CM, Ildefonso CJ, et al. Systemic treatment with a 5HT1a agonist induces anti-oxidant protection and preserves the retina from mitochondrial oxidative stress. *Exp Eye Res*. 2015;140:94–105.

Investigative Ophthalmology & Visual Science